

SUR-FeatNet: Predicting the Satisfied User Ratio Curve for Image Compression with Deep Feature Learning

Hanhe Lin¹ · Vlad Hosu¹ · Chunling Fan² · Yun Zhang² · Yuchen Mu³ ·
Raouf Hamzaoui⁴ · Dietmar Saupe¹

Received: date / Accepted: date

Abstract The Satisfied User Ratio (SUR) curve for a lossy image compression scheme, e.g., JPEG, gives the distribution function of the Just Noticeable Difference (JND), the smallest distortion level that can be perceived by a subject when a reference image is compared to a distorted one. A sequence of JNDs can be defined with a suitable successive choice of reference images. We propose the first deep learning approach to predict SUR curves. We show how to exploit maximum likelihood estimation and the Kolmogorov-Smirnov test to select a suitable parametric model for the distribution function. We then use deep feature learning to predict samples of the SUR curve and apply the method of least squares to fit the parametric model to the predicted samples. Our deep learning approach relies on a Siamese Convolutional Neural Networks (CNN), transfer learning, and deep feature learning, using pairs consisting of a reference image and compressed image for training. Experiments on the MCL-JCI dataset showed state-of-the-art performance. For example, the mean Bhattacharyya distances between the predicted and ground truth first, second, and third JND distributions were 0.0810, 0.0702, and 0.0522, respectively, and the corresponding average absolute differences of the peak

signal-to-noise ratio at the median of the distributions were 0.56, 0.65, and 0.53 dB.

1 Introduction

Image compression is typically used to meet constraints on transmission bandwidth and storage space. The quality of a compressed image is quantitatively determined by encoding parameters, e.g., the Quality Factor (QF) in JPEG compression. When images are compressed, artifacts such as blocking and ringing may appear and affect the visual quality experienced by the users. The Satisfied User Ratio (SUR) is the fraction of users that do not perceive any distortion when comparing the original image to its compressed version. The constraint on the SUR may vary according to the application.

Determining the relationship between the encoding parameter and the SUR is a challenging task. The conventional method consists of three steps. First, the source image is compressed multiple times at different bitrates. Next, a group of subjects are asked to identify the smallest distortion level that they can perceive. A subject cannot notice the distortion until it reaches a certain level. This Just Noticeable Difference (JND) level is different from one subject to another due to individual variations in the physiological and visual attention mechanisms. Finally, the overall SUR for the image is obtained by statistical analysis. Following this procedure, several subjective quality studies were conducted and yielded JND-based image and video databases, e.g., MCL-JCI [12], MCL-JCV [23], VideoSet [25], SIAT-JSSI [5], and SIAT-JASI [5]. Subjective visual quality assessment studies are reliable but time-consuming and

Funded by the Deutsche Forschungsgemeinschaft (DFG, German Research Foundation) – Project-ID 251654672 – TRR 161 (Project A05).

¹ Department of Computer and Information Science, University of Konstanz, Germany. E-mail: hanhe.lin@uni-konstanz.de

² Shenzhen Institutes of Advanced Technology, Chinese Academy of Sciences, China.

³ School of Engineering, University of Edinburgh, UK.

⁴ School of Engineering and Sustainable Development, De Montfort University, UK.

expensive. In contrast, objective, i.e., algorithmic, SUR estimation can work in real-time and at no extra cost.

In recent years, deep learning has made tremendous progress in computer vision tasks such as image classification [22] [8], object detection [21] [17], and Image Quality Assessment (IQA) [2] [10] [26]. Instead of carefully designing handcrafted features, deep learning-based methods automatically discover representations from raw image data that are most suitable for the specific tasks, and can improve the performance significantly.

Inspired by these works, we propose a novel deep learning approach to predict the relationship between the SUR and the encoding parameter (or distortion level) for compressed images. Given a pristine image and its distorted versions, we first use a Siamese network to predict the SUR at each distortion level. Then we apply the least squares method to fit a parametric model to the predicted values and use the graph of this model as SUR curve.

The main contributions of our work are as follows:

1. We propose a deep learning architecture to predict samples of the SUR curves of compressed images automatically, followed by a regression step yielding a parametric SUR model. To the best of our knowledge, this is the first work of its kind.
2. We exploit maximum likelihood estimation (MLE) and the Kolmogorov-Smirnov (K-S) test to select the most suitable parametric distribution for SUR modelling instead of using the normal distribution as a default like all previous works.
3. We improve the performance of our model by using transfer feature learning from a similar prediction task. We first train the proposed model independently on an IQA task. Given the images for SUR prediction, we extract Multi-Level Spatially Pooled (MLSP) [9] features from the learnt model, on which a shallow regression network is further trained to predict the SUR value for a given image pair.

This article is an extension of our work in [4]. Our new contributions are as follows. First, we optimize the proposed architecture and apply feature learning instead of a fine-tuning approach, significantly decreasing computational cost and improving performance. Second, we use MLE and the K-S test to select the JND distribution model. Finally, we conduct more experiments to prove the efficiency of our model, providing results for not only the first JND, but for the second and third JNDs as well.

2 Definitions

We consider a lossy image compression scheme that produces monotonically increasing distortion magnitudes as a function of an encoding parameter. The metric for the distortion magnitude may be the mean squared error, and the encoding parameter is assumed to take only a finite number of values. For example, in JPEG, the encoding parameter is the quality factor $QF \in \{1, \dots, 100\}$. A value of QF corresponds to the distortion level $n = 101 - QF$, where $n = 1$ is the smallest and $n = 100$ is the largest distortion level.

Definition 1 (*k*th JND). For a given pristine image $I[0]$, we associate distorted images $I[n]$, $n = 1, \dots, N$ corresponding to distortion levels $n = 1, \dots, N$. Let JND_0 be the (trivial) random variable with $\mathbb{P}(JND_0 = 0) = 1$. The *k*th JND, which we denote by JND_k , $k > 1$, is a random variable whose value is the smallest distortion level that can be perceived by an observer when the image $I[JND_{k-1}]$ is compared to the images $I[n]$, $n > JND_{k-1}$. The median of the probability distribution of JND_k is also called the *k*th JND when there is no risk of confusion.

Samples of the JNDs can be generated iteratively. The original pristine image $I[0]$ serves as the first anchor image and the increasingly distorted images $I[n]$, $n = 1, 2, \dots$ are displayed sequentially together with the anchor image until a distortion can be perceived. This yields a sample of the first JND. This first image with a noticeable distortion then replaces the anchor image, to be compared with the remaining distorted images sequentially until again a noticeable difference is detected, yielding a sample of the second JND, and so on. For simplicity, by JND we will refer to the random variable JND_k or to its median when there is no risk of confusion.

The set of random variables $\{JND_k, k \geq 1\}$ in Definition 1 is a discrete finite stochastic process. The number of (non-trivial) JNDs of the stochastic process depends on the image sequence on hand. It is limited by the smallest number of JNDs that a random observer is able to perceive for the given image sequence. In practical applications, the first JND is the most important one, and at the following JNDs the image quality is degraded multiple times from the original which implies that a satisfactory usage of the corresponding images may be very limited. In this paper, we have considered only the first three JNDs, which was also the choice made in [25].

Definition 1 is intended for sequences of increasingly distorted images, and the prototype application is given by image compression with decreasing bitrate. However, it can also be applied to other media like sequences of video clips or, more generally, to sequences of perceptual stimuli of any kind. Moreover, these sequences need not be sequences with increasing distortion. JNDs may also be useful, for example, to study the effect of parameter-dependent image enhancement methods.

Although there are many publications on just noticeable difference, especially in psychophysics [6], the notion of a sequence of JNDs as considered in this paper was only introduced recently in [16]. In that contribution, an empirical study for 5 sequences of compressed images and video clips was carried out, with 20 subjects contributing their sequences of JND samples for each set of stimuli. In the followup paper [12], a larger dataset of 50 source images was introduced, including subjective tests with 30 participants, and providing the dataset MCL-JCI, that we are using for our studies here. Neither of the mentioned contributions gave a formal definition of JNDs. However, the experimental protocols suggest that in these papers the JND random variables were sampled in the spirit of Definition 1.

In a later paper [25], the k th JND for $k > 1$ was obtained differently, by using the same anchor image for all observers. This anchor image was chosen as the one corresponding to the 75% quantile of the previous JND, i.e., the point at which the fraction of observers that cannot perceive a noticeable difference drops below 75%.

Definition 2 (SUR function and curve). The SUR function is the complementary cumulative distribution function (CCDF) of the JND. The graph of this function is called the SUR curve.

The SUR function, which we denote by $\text{SUR}(\cdot)$, gives the proportion of the sample population for which the JND is greater than a given value. That is,

$$\text{SUR}(x) = \mathbb{P}(\text{JND} > x).$$

Since the range of the JND is discrete (i.e., integers $\{1, 2, \dots, N\}$), the SUR function is a monotonically decreasing step function.

The SUR curve can be used to determine the highest distortion level for which a given proportion of the population is satisfied, in the sense that it cannot perceive a distortion. Formally, we apply the definition of the SUR function and curve also for the second and third JND, although for these cases, an interpretation as a proportion of “satisfied” users is not appropriate.

If we set the satisfied user ratio to 0.75, as suggested in [24], we can define the 75% SUR as follows:

Definition 3 (75% SUR). The 75% SUR is the largest integer in the set $\{1, 2, \dots, N\}$ for which the SUR function is greater than or equal to 0.75,

$$75\% \text{ SUR} = \max\{d \in \{1, \dots, N\} \mid \text{SUR}(d) \geq 0.75\}.$$

The notion of 75% SUR can be extended to that of $p\%$ SUR in a straightforward way. Likewise, the JND, taken as the median of a JND distribution (i.e., the distortion level at 50% SUR) can also be defined for other percentages, if desired.

3 Related works

Existing research on JND can be classified into three main areas: subjective quality assessment studies to collect JND samples, mathematical modeling of the JND probability distribution and SUR function, and prediction of the probability distribution of the JND and the SUR curve for a given image or video.

3.1 Subjective quality assessment

Jin *et al.* [12] conducted subjective quality assessment tests to collect JND samples for JPEG compressed images and built a JND-based image dataset called MCL-JCI. The tests involved 150 participants and 50 source images. With JND samples for a given image collected from 30 subjects, they found that humans can distinguish only a few distortion levels (5 to 7). Since subjective tests are time-consuming and expensive, a binary search algorithm was proposed to speed up the annotation procedure.

Wang *et al.* [23] conducted subjective tests on JND for compressed videos using H.264/AVC coding. They collected JND samples from 50 subjects, building a JND-based video dataset called MCL-JCV.

Wang *et al.* [25] built a large-scale JND video dataset called VideoSet for 220 5-s source videos in four resolutions (1080p, 720p, 540p, 360p). Distorted versions of the videos were obtained with H.264/AVC compression. To obtain the JND value for a given subject, they used a modified binary search procedure comparable to the ones adopted in [12] and [23]. For each subject, the values of the first three JNDs were collected.

Fan *et al.* [5] studied the JND of symmetrically and asymmetrically compressed stereoscopic images for

JPEG2000 and H.265 intra-coding. They generated two JND-based stereo image datasets, one for symmetric compression and one for asymmetric compression.

3.2 Mathematical modeling of JND and SUR

In [12], it was assumed that the JND distribution for an image is a Gaussian mixture with a finite number of components. The parameters of the Gaussian mixture model (GMM) were determined with the Expectation Maximization algorithm. The number of components of the GMM was determined with the Bayesian information criterion.

In [23] and [25], a normal distribution was used to model the three first JNDs. In [25], the Jarque-Bera test was used to check whether the JND samples have the skewness and kurtosis matching a normal distribution. Almost all tested videos passed the test.

In [5], we assumed that the JND on the QF scale was normally distributed but also noted that an empirical test (β_2 test [20]) found that only 29 of the 50 source images passed the normality test. In Section 4.2, we show that other models are more suitable and propose a method to select one.

3.3 Prediction of JND and SUR

Huang *et al.* [11] propose a Support Vector Regression (SVR)-based model to predict the mean value of the JND for HEVC encoded videos. They exploit the masking effect and a Spatial Temporal Sensitive Map based on spatial, saliency, luminance, and temporal information.

Wang *et al.* [24] also use SVR to predict the SUR curve. The SVR is fed a feature vector consisting of the concatenation of two feature vectors. The first one is based on the computation of Video Multimethod Assessment Fusion (VMAF) [14] quality indices on spatial-temporal segments of the compressed video, while the second one is based on spatial randomness and temporal randomness features that measure the masking effect in the corresponding segments of the source video. For the VideoSet, the average prediction error at the 75% SUR between the predicted quantization parameter (QP) value and the ground truth QP value was found to be 1.218, 1.273, 1.345, and 1.605 for resolutions 1080p, 720p, 540p, and 360p, respectively.

Hadizadeh *et al.* [7] build an objective predictor (binary classifier) to determine whether a reference image is perceptually distinguishable from a version contaminated with noise according to a JND model. Given a reference image and its noisy version, they use sparse

coding to extract a feature vector and feed it into a multi-layer neural network for the classification. The network is trained on a dataset obtained through subjective experiments with 15 subjects and 999 reference images. The predictor achieves a classification accuracy of about 97% on this dataset.

Liu *et al.* [18] propose a deep learning technique to predict the JND for image compression. JND prediction is seen as a multi-class classification problem, which is converted into several binary classification problems. The binary classifier is based on deep learning and predicts whether a distorted image is perceptually lossy with respect to a reference. A sliding window technique is used to deal with inconsistencies of the multiple binary classification. Experimental results for MCL-JCI show that the absolute prediction error of the proposed model is 0.79 dB PSNR on average.

4 Deep learning for SUR prediction

4.1 Structure of training data

We need to predict SUR curves that are calculated from subjective JND studies, given a reference image and a distortion type, e.g., JPEG compression. In order to train a good machine learning model, we considered a few ways to present the available information during training. With respect to the inputs, we could present one (the reference) or more input images (reference and distorted images) to the model. The output has to be a representation of the SUR function.

With regard to the outputs, for a reference image $I[0]$ and its distorted versions $I[1], \dots, I[N]$ the SUR curve can be represented as $SUR(1), \dots, SUR(N)$. The SUR function can be calculated from the empirical CCDF, or by first fitting an appropriate analytical distribution to the subjective data. In the latter case, the analytical representation can be sampled similarly to the empirical SUR or the model can be trained to predict the parameters of the analytical CCDF.

For the inputs of the model, if we attempted to predict a representation of the SUR curve from a single reference image, we would be ignoring information about the particular type of degradation that was applied to images in the subjective study. The model is expected to learn better when both the reference and its distorted version(s) are considered. Ideally we should provide the model with the reference and all the distorted images as inputs. In this way, using an appropriate learning method the model has all the information that participants in the experiments had, and is expected to perform the best. However, in this formulation the problem is more difficult to solve. We simplify it by inputting

pairs of images: a reference $I[0]$ and a distorted version $I[k]$, $k \in \{1, \dots, N\}$. In this case we have two options for the outputs: 1. either predict the representation of the entire SUR curve (sampled, or parametric) or 2. predict the corresponding $\text{SUR}(k)$ value. In both cases (1. and 2.), as predictions are independent of each other, the pairwise predictions need to be aggregated into a single SUR curve over all distortion levels for a given reference.

We chose to do pair-based prediction of sampled analytical SUR functions. Predicting the empirical samples of the SUR does not perform as well as predicting the sampled analytical SUR. This is probably due to the denoising effect of first mapping a distribution to the subjective data. Each sample of the SUR is independently predicted, and then the overall SUR is estimated from the samples by least-squares fitting.

4.2 Modeling the SUR function

We now see the JND as a continuous random variable that has a mathematical form defined by parameters. Its CCDF is the SUR function. To select the most suitable distribution for a given dataset of samples, we use maximum likelihood estimation (MLE) and the Kolmogorov-Smirnov (K-S) test. MLE allows us to estimate the parameters of the probabilistic models and also to rank different models according to increasing negative log-likelihood, averaged over the source images in the dataset. For a given distribution model and a set of corresponding samples, the K-S test can be applied for the null hypothesis that the JND samples were drawn from the model at a specified significance level (5% in our experimental settings). This allows us to rank the models according to the number of times the null hypothesis was rejected.

We considered the 20 parametric continuous probability distribution models that are available in Matlab and fitted them to JND samples, expressed in terms of distortion levels and also in the reverse orientation, i.e., with respect to the corresponding JPEG quality factors QF. In both cases, we found that the Generalized Extreme Value (GEV) distribution was the most suitable model for the first three JNDs.

The probability density function (PDF) of the GEV distribution is given by

$$f(x|\xi, \mu, \sigma) = \frac{1}{\sigma} \exp(-z^{-\frac{1}{\xi}}) z^{-1-\frac{1}{\xi}} \quad (1)$$

where $x \in \mathbb{R}$ satisfies

$$z = 1 + \xi \frac{x - \mu}{\sigma} > 0$$

Here, $\xi \neq 0$, μ , and σ are called shape parameter, location parameter, and scale parameter, respectively.

For example, for the 50 source images in the MCL-JCI dataset [12] and their QF data, the GEV distribution ranked second in terms of the negative log-likelihood and first in terms of the K-S test for the first JND. In contrast, the Gaussian distribution, ranked 12th for the negative log-likelihood criterion and 9th for the K-S test (Table 1). Since convergence of MLE was better for the QF data than for the distortion level data, we built our models based on the QF data. That is, we used the PDF

$$f_Y(y) = f_X(101 - y | \xi, \mu, \sigma) \quad (2)$$

to model the JND distribution, where f_X is the PDF of the GEV that models the QF data. Note that f_Y is not the PDF of a GEV distribution. Finally, the CCDF of f_Y ,

$$\bar{F}(y | \xi, \mu, \sigma) = 1 - \int_{-\infty}^y f_Y(s | \xi, \mu, \sigma) ds,$$

served as a model for the SUR function, where we have copied the GEV parameters of f_X in the notation of f_Y and \bar{F} for convenience.

Fig. 1(a) shows the histogram of the first JND for the fifth image in the MCL-JCI dataset, the corresponding empirical SUR curve, the model obtained with MLE of the GEV distribution for the QF data, the corresponding SUR curve, and the 75% SUR. Fig. 1(b) and Fig. 1(c) show similar results for the second and third JND, respectively. Fig. 2 shows the results for the 14th image in the MCL-JCI dataset, highlighting the 50% SUR instead of the 75% SUR.

4.3 Problem definition

The regression problem for predicting SUR curves can be formulated as follows. Let $I_1[0], I_2[0], \dots, I_K[0]$ be a training set of K pristine reference images. For each reference image $I_k[0]$, $k \in \{1, \dots, K\}$, we associate the N distorted images $I_k[n]$, $n = 1, \dots, N$ corresponding to the N distortion levels $n = 1, \dots, N$.

Problem. Let $\text{SUR}_k(\cdot)$, $k = 1, \dots, K$, denote the SUR function of image $I_k[0]$ and its sequence of distorted images $I_k[1], \dots, I_k[N]$. Find a deep regression model f_θ , parameterized by θ , such that

$$f_\theta(I_k[0], I_k[n]) \approx \text{SUR}_k(n)$$

for $k = 1, \dots, K$, $n = 1, \dots, N$.

Table 1 Ranking of the distribution models according to negative loglikelihood of MLE and K-S test for the 50 source images in the MCL-JCI dataset [12]. The models used are Half-normal (1), Rayleigh (2), Exponential (3), Generalized Extreme Value (4), Generalized Pareto (5), Stable (6), tLocation Scale (7), Birnbaum-Saunders (8), Extreme Value (9), Gamma (10), Logistic (11), Loglogistic (12), LogNormal (13), Nakagami (14), Normal (15), Poisson (16), Rician (17), Weibull (18). Results for two other models available in Matlab, beta distribution and Burr distribution, are not included as fitting the JND samples with the distributions was not possible.

Models		1	2	3	4	5	6	7	8	9	10	11	12	13	14	15	16	17	18
First JND	loglikelihood	16	14	17	2	13	3	1	4	15	7	11	6	5	8	12	18	10	9
	K-S test	14	11	14	1	13	1	6	7	10	5	3	2	4	8	9	12	7	5
Second JND	loglikelihood	16	13	17	1	14	5	10	2	15	4	11	6	3	7	12	18	9	8
	K-S test	9	5	8	1	7	1	1	2	4	1	1	1	2	2	3	6	2	2
Third JND	loglikelihood	16	13	17	1	14	5	10	2	15	4	11	6	3	7	12	18	9	8
	K-S test	7	4	8	1	6	1	1	1	3	1	1	1	1	2	2	5	1	1

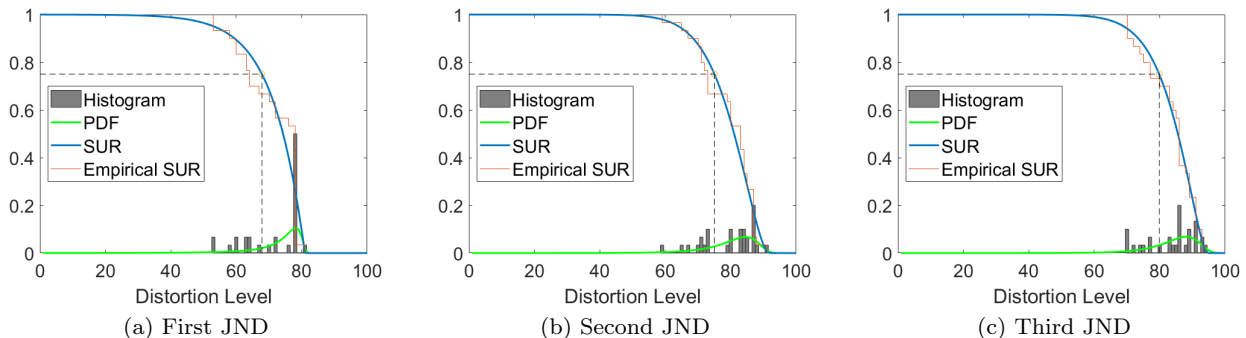


Fig. 1 SUR curve and 75% SUR of the first three JNDs. The data is for the fifth source image in the MCL-JCI dataset [12].

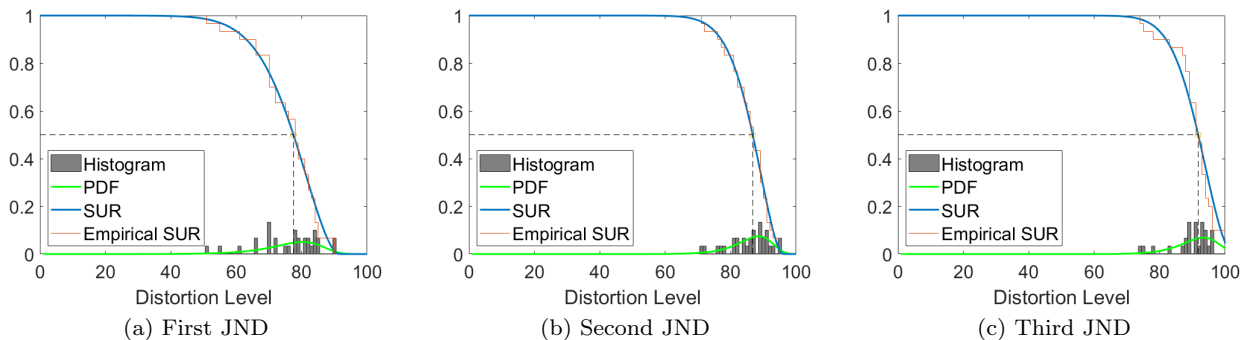


Fig. 2 SUR curve and 50% SUR of the first three JNDs. The data is for the 14th source image in the MCL-JCI dataset [12].

4.4 Proposed model

Subjective studies are usually time-consuming and expensive, which limits JND datasets to relatively small size. With such small data, training a deep model from scratch may be prone to overfitting. To address this limitation we propose a two-stage model that applies transfer learning and feature learning, as depicted in Fig. 3.

In the first stage (Fig. 3a), a pair of images, namely a pristine image $I_k[0]$ and a distortion version $I_k[n]$, are fed into a Siamese network that uses an Inception-V3 [22] CNN body with shared weights. The network body is truncated, such that the global average pooling (GAP) layer and the final fully-connected layer are

removed. Each branch of the Siamese network yields a stack of 2,048 feature maps. The feature maps are passed through a GAP layer, which outputs a 2,048-dimensional feature vector \mathbf{f}_{gap} for each branch. Then we calculate $\Delta\mathbf{f}_{\text{gap}}$, corresponding to feature vector differences between the distorted images $I_k[n]$ and the pristine image $I_k[0]$, i.e.,

$$\Delta\mathbf{f}_{\text{gap}} = \mathbf{f}_{\text{gap}}(I_k[0]) - \mathbf{f}_{\text{gap}}(I_k[n]).$$

By concatenating the two feature vectors $\mathbf{f}_{\text{gap}}(I_k[0])$, $\mathbf{f}_{\text{gap}}(I_k[n])$ and the feature difference vector $\Delta\mathbf{f}_{\text{gap}}$, we obtain a 6,144 dimensional vector. The latter is passed to three fully connected (FC) layers with 512, 256, and 128 neurons, respectively, where each FC layer is followed by a dropout layer (0.25 ratio) to avoid over-

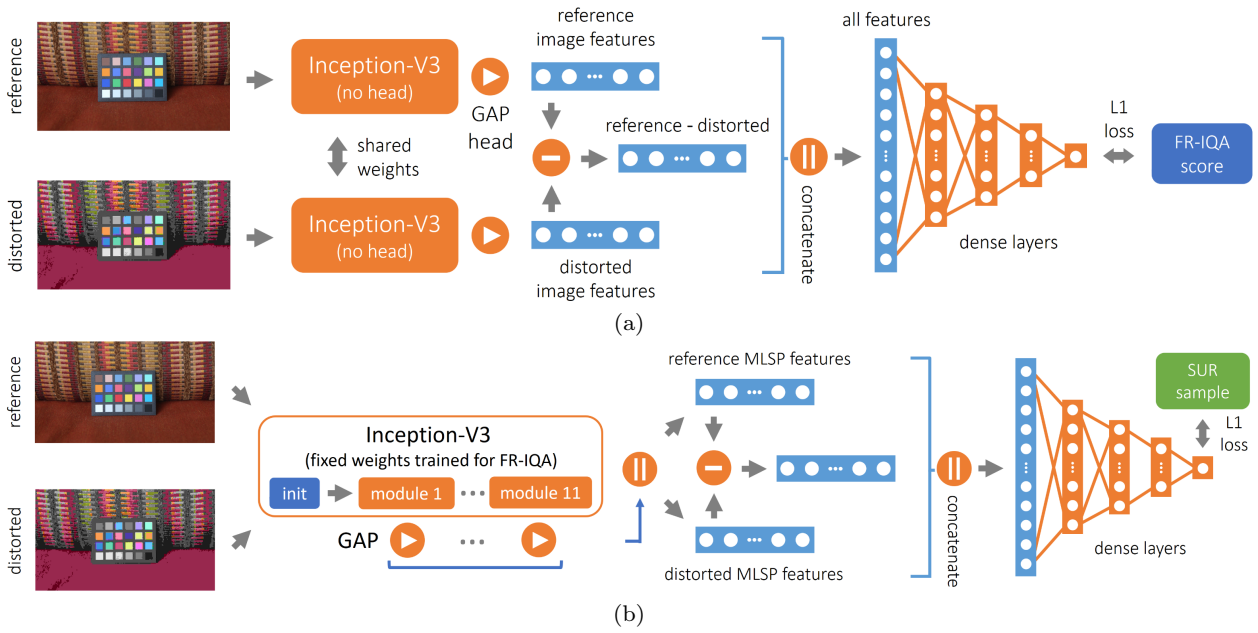


Fig. 3 SUR-FeatNet architecture for prediction of the satisfied user ratio curve. In the first stage (a), a Siamese CNN is used to predict an objective quality score of a reference image and its distorted version, which is similar to SUR prediction task (b) and allowed us to train on a large-scale dataset to address overfitting. In the second stage (b), MLSP features of a reference image and its distorted version were extracted and fed into a shallow regression network that was used to predict SUR values.

fitting. The output layer is linear with one neuron to predict a quality score of the distorted image $I_k[n]$, obtained from a fixed Full-Reference (FR)-IQA method.

In the second stage (Fig. 3b), we keep the weights fixed in the Inception-V3 body as trained in the first stage. A reference and a distorted image are presented to the Inception-V3 body, and for each of them Multi-Level Spatially Pooled (MLSP) [9] features \mathbf{f}_{mlsp} with 10,048 components each are extracted. As in the first stage, we concatenate $\mathbf{f}_{\text{mlsp}}(I_k[0])$, $\mathbf{f}_{\text{mlsp}}(I_k[n])$, and $\Delta\mathbf{f}_{\text{mlsp}} = \mathbf{f}_{\text{mlsp}}(I_k[0]) - \mathbf{f}_{\text{mlsp}}(I_k[n])$. The concatenated 30,144-dimensional feature vector is passed to an FC head to predict the SUR value. This FC head has the same structure as the FC head in the first stage.

Let (I_r, I_d, q) be an item of the training data, where I_r and I_d are the reference image and its distorted version, and q corresponds to the FR-IQA score in the first stage and the SUR value in the second stage. Our objective is to minimize the mean absolute error (MAE), or L1 loss function:

$$L_{\text{MAE}} = |f_{\theta}(I_r, I_d) - q|. \quad (3)$$

Our proposed model, called SUR-FeatNet, has the following properties. We first train a deep model to predict the FR-IQA score of a distorted image relative to its pristine original. This is similar to predicting a SUR value and therefore the features learned in the first stage are expected to be useful for predicting SUR values in the second stage. As it is very convenient to generate

distorted images given a large-scale set of pristine reference images and to estimate their quality score by an FR-IQA method, training a deep model on a large-scale image set to address overfitting becomes feasible.

Second, training on these “locked-in” MLSP features in the second stage instead of fine-tuning a very large deep network not only reduces computational time, but also prevents forgetting previously trained information, which may lead to a better performance on a small dataset.

5 Prediction of the SUR curve and the JND

For any source image $I[0]$, together with its distorted versions $I[1], \dots, I[N]$, a sequence of predicted satisfied user ratios $\text{SUR}(1), \dots, \text{SUR}(N)$ is obtained from the network. Assuming that the JND of the QF data follows a GEV distribution, we estimate the shape parameter ξ , the location parameter μ , and the scale parameter σ by least squares fitting,

$$(\hat{\xi}, \hat{\mu}, \hat{\sigma}) = \arg \min_{\xi, \mu, \sigma} \sum_{n=1}^N |\bar{F}(n | \xi, \mu, \sigma) - \text{SUR}(n)|^2.$$

The fitted SUR curve is given by $\bar{F}(n | \hat{\xi}, \hat{\mu}, \hat{\sigma})$.

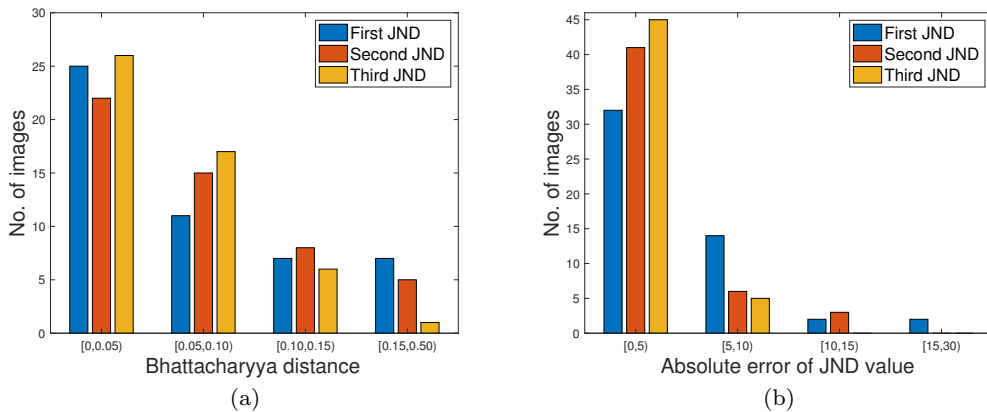


Fig. 4 Statistics of experimental results. (a) Histogram of Bhattacharyya distance between predicted JND distribution and ground truth JND distribution. (b) Histogram of the absolute error between predicted JND (50% SUR) and ground truth JND (50% SUR). The GEV distribution is used as distribution model.

6 Experiment

6.1 Setup

In our experiments, we used the MCL-JCI dataset [12] to evaluate the performance of the proposed method. The dataset contains 50 pristine images with a resolution of 1920×1080 . Each pristine image was encoded 100 times by a JPEG encoder with QF decreasing from 100 to 1, corresponding to distortion levels 1 to 100. Thus, there are 5,050 images in total.

The annotation provided for the image sequences in MCL-JCI and for each of the $M = 30$ participants of the study [12] is the QF value corresponding to the first JND (and also those of the second, third, etc.). For each source image $I_k[0]$ ($k = 1, \dots, 50$) in the MCL-JCI dataset, we modeled its SUR function for the given JND samples, according to the GEV distribution (Eq. (1)). Finally, we sampled the fitted SUR model to derive the target values $SUR_k(n)$, $k = 1, \dots, 50$, $n = 1, \dots, 100$ for the deep learning algorithm.

k -fold ($k = 10$) cross validation was used to evaluate the performance. Specifically, the dataset was divided into 10 subsets, each containing five source images and all 500 distorted versions of them. Each time, one subset was kept as a test set, and the remaining nine subsets were used for training and validation. The overall result was the average of 10 test results.

The Adam optimizer [13] was used to train SUR-FeatNet with the default parameters $\beta_1 = 0.9$, $\beta_2 = 0.999$, and a custom learning rate α . We set $\alpha = 10^{-5}$ and trained for 30 epochs. In the training process, we monitored the MAE loss on the validation set and saved the best performing model. Our implementation used the Python Keras library with Tensorflow as a backend

[3] and ran on two NVIDIA Titan Xp GPUs, where the batch size was set to 16.

6.2 Strategies to address overfitting

For the first stage of our model, we used the Konstanz Artificially Distorted Image quality Set (KADIS-700k) [15]. This dataset has 140,000 pristine images, with five degraded versions each, where the distortions were chosen randomly out of a set of 25 distortion types. We used a full-reference IQA metric to compute the objective quality scores for all the pairs. For this purpose we chose MDSI [19] as it was reported as the best FR-IQA metric when evaluating on multiple benchmark IQA databases. As KADIS-700k is a large-scale set, we only trained for five epochs before MLSP feature extraction.

In addition to transfer learning in the first stage, we applied image augmentation in the second stage to help avoid overfitting. Each image of the MCL-JCI dataset was split into four non-overlapping patches with a resolution of 960×540 . We also cropped one patch of the same resolution from the center of the image. The SUR values for the patches were set to be equal to those of their source images. With this image augmentation, we had 25,250 annotated patches.

After training the networks with these training sets, SUR values were predicted for the test set. To predict the SUR of a distorted image, predictions for its five corresponding patches were generated by the network and averaged.

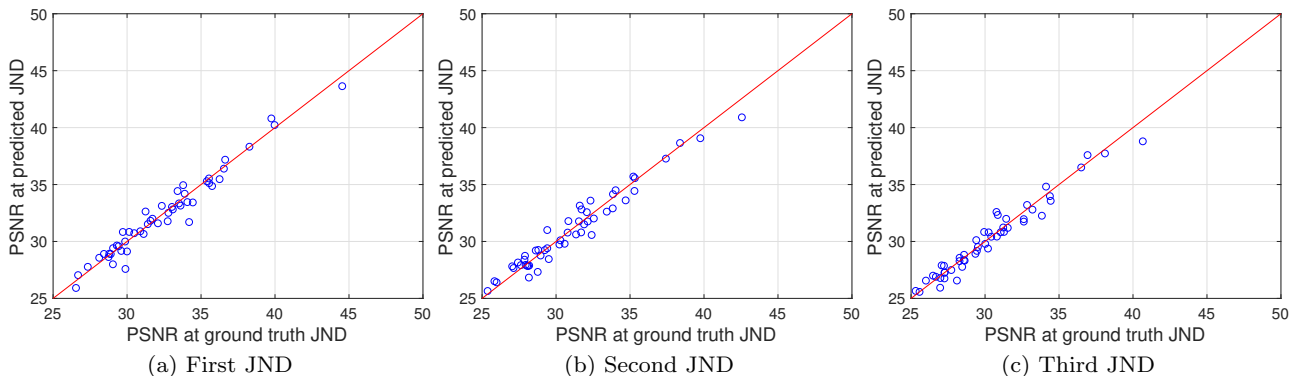


Fig. 5 PSNR comparison between the ground truth JNDs and predicted JNDs at first JND (a), second JND (b), and third JND (c). The corresponding PLCCs are 0.9782, 0.9758, and 0.9783.

6.3 Results and analysis

Three metrics were used to evaluate the performance of SUR-FeatNet: MAE of the JNDs (medians of the JND distributions), MAE of the Peak Signal-to-Noise Ratio (PSNR) at the JNDs, and Bhattacharyya distance [1] between the predicted and ground truth JND distributions of type GEV. The ground truth GEV parameters were obtained by using MLE to fit a GEV distribution to the MCL-JCI QF values.

We first compared the performance of the following four learning schemes.

- (1) *Fine-tune (ImageNet)*. In the first scheme, we used the architecture in the first stage (Fig. 3a). Its CNN body was initialized with the pre-trained weights on ImageNet and FC layers were initialized with random weights. With the initialized weights, the network was fine-tuned for SUR prediction using the MCL-JCI dataset.
- (2) *Fine-tune (KADIS-700k)*. The second scheme used the same architecture and same initialized weights as the first scheme. However, it was first fine-tuned on KADIS-700k to predict FR-IQA quality scores before it was fine-tuned on MCL-JCI dataset.
- (3) *MLSP (ImageNet)*. In the third scheme, we trained a shallow regression network for SUR prediction based on MLSP features, which were extracted from a pre-trained network on ImageNet.
- (4) *MLSP (KADIS-700k)*. The fourth scheme, which is used by our approach, trained the same regression network as the third scheme. However, its MLSP features were extracted from fine-tuned weights on KADIS-700k instead of ImageNet.

Table 2 shows the performance of the four schemes for the first JND. Clearly, transfer learning from the image classification domain (ImageNet) to the quality assessment domain (KADIS-700k), together with MLSP feature learning, outperforms the remaining schemes.

Scheme	Bhattacharyya distance	Δ JND	Δ PSNR (dB)
1. Fine-tune (ImageNet)	0.1244	5.86	0.74
2. Fine-tune (KADIS-700k)	0.0936	5.17	0.64
3. MLSP (ImageNet)	0.0949	5.22	0.64
4. MLSP (KADIS-700k)	0.0810	4.53	0.56

Table 2 Performance comparison for the first JND with different learning schemes.

Tables 5, 6, and 7 present the detailed results of the first, second, and third JND for each image sequence. Fig. 4 shows the statistics. For all three JNDs, more than 75% of the images have a Bhattacharyya distance smaller than 0.1 (Fig. 4(a)). With respect to first, second, and third JND, the absolute error in JND was less than 5 for 32, 41, and 45 images, respectively (Fig. 4(b)). For more than 90% of the images, the absolute error in JND was smaller than 10. Fig. 5 compares the PSNR at ground truth JND and predicted JND for the first, second, and third JNDs. The Pearson Linear Correlation Coefficient (PLCC) was very high, reaching 0.9782, 0.9758, and 0.9783, respectively.

JND	Bhattacharyya distance	Δ JND	Δ PSNR (dB)
First	0.0810	4.53	0.56
Second	0.0702	3.28	0.65
Third	0.0522	2.07	0.53

Table 3 SUR-FeatNet performance for the first three JNDs.

Fig. 6 shows the best two predictions, sorted according to the mean Bhattacharyya distance over the three JNDs. The best prediction result was for image 35, with absolute JND errors of 0.30, 0.46, and 0.15, Bhattacharyya distances of 0.0073, 0.0073, and 0.0052, and PSNR differences at the JNDs of 0, 0, and 0.3 dB for the first, second, and third JND, respectively.

The prediction results for a few images were not as good. For example, Fig 7 presents the worst two pre-

dictions. The worst prediction was for image 12, which had absolute JND errors of 27.13, 12.34, and 2.02, Bhattacharyya distances of 0.4884, 0.2373, and 0.0167, and PSNR differences at the JND of 2.49, 1.84, and 0.37 for the first, second, and third JND, respectively. This may be because the size and diversity of the training set are too small for the deep learning algorithm. We expect that this problem can be overcome by training on a large-scale JND dataset.

The overall performance of SUR-FeatNet is displayed in Table 3. The mean Bhattacharyya distances between the predicted and the ground truth first, second, and third JND distributions were only 0.0810, 0.0702, and 0.0522, respectively.

6.4 Comparison with previous work

SUR-FeatNet outperformed the state-of-the-art PW-JND model of Liu *et al.* [18] for the first and second JND, see Table 4, except for the mean absolute error of the predicted distortion level of the second JND. There are no results listed in [18] for the third JND. Note, that in [18] the ground truth JNDs are slightly different from those used for SUR-FeatNet, as they had been taken from the model in [12] (Table 2). One advantage of our method compared to the work in [18] is that it can predict the distortion level at arbitrary percentiles (e.g., at the 75% SUR).

SUR-FeatNet also showed a better performance when predicting the 75% SUR for the first JND in the MCL-JCI dataset, compared to our previous model SUR-Net [4] (Table 4).

Method	First JND		Second JND		75%SUR	
	MAE	Δ PSNR (dB)	MAE	Δ PSNR (dB)	MAE	Δ PSNR (dB)
PW-JND [18]	8.7	0.82	3.14	0.76	–	–
SUR-Net [4]	5.22	0.63	–	–	6.73	0.69
SUR-FeatNet	4.53	0.56	3.28	0.65	5.45	0.58

Table 4 Performance comparison with the state-of-the-art PW-JND model [18] and SUR-Net [4]. The MAE refers to the error in distortion levels.

7 Conclusion and future work

We proposed a deep learning approach to predict the SUR curve for compressed images. In a first stage, pairs of images (a reference and a distorted one) are fed into a Siamese CNN to predict their objective quality score. In a second stage, extracted MLSP features are fed into a shallow regression network to predict the SUR value of a given image pair. The proposed approach can be

easily generalized to predict the SUR curves for images compressed with other coders. We provided results for the 50% and 70% SUR. Results for other satisfied user ratios can be obtained in a similar way. Given a target percentage of satisfied users, the predicted SUR curve can be used to determine the JPEG quality factor QF that provides a compressed image, which is indistinguishable from the original for these users, thereby saving bit rate without the need for subjective visual quality tests.

To improve the performance of our model, one could predict the parameters of the analytical distribution given each source image and all its distorted versions. However, such an approach requires more data to train, which goes in another research direction, namely, how to efficiently create a large-scale JND database.

Conflict of interest

The authors declare that they have no conflict of interest.

References

- Bhattacharyya, A.: On a measure of divergence between two statistical populations defined by their probability distributions. *Bulletin of the Calcutta Mathematical Society* **35**, 99–109 (1943)
- Bosse, S., Maniry, D., Müller, K.R., Wiegand, T., Samek, W.: Deep neural networks for no-reference and full-reference image quality assessment. *IEEE Transactions on Image Processing* **27**(1), 206–219 (2018)
- Chollet, F., et al.: Keras. <https://keras.io> (2015)
- Fan, C., Lin, H., Hosu, V., Zhang, Y., Jiang, Q., Hamzaoui, R., Saupe, D.: SUR-Net: Predicting the satisfied user ratio curve for image compression with deep learning. In: 2019 Eleventh International Conference on Quality of Multimedia Experience (QoMEX), pp. 1–6. IEEE (2019)
- Fan, C., Zhang, Y., Zhang, H., Hamzaoui, R., Jiang, Q.: Picture-level just noticeable difference for symmetrically and asymmetrically compressed stereoscopic images: Subjective quality assessment study and datasets. *Journal of Visual Communication and Image Representation* **62**, 140–151 (2019)
- Gescheider, G.A.: *Psychophysics: The Fundamentals*. Psychology Press (2013)
- Hadizadeh, H., Reza Heravi, A., Bajic, I.V., Karami, P.: A perceptual distinguishability predictor for JND-noise-contaminated images. In: *IEEE Transactions on Image Processing*, pp. 1–15 (2018)
- He, K., Zhang, X., Ren, S., Sun, J.: Deep residual learning for image recognition. In: *IEEE Conference on Computer Vision and Pattern Recognition (CVPR)*, pp. 770–778 (2016)
- Hosu, V., Goldlucke, B., Saupe, D.: Effective aesthetics prediction with multi-level spatially pooled features. In: *Proceedings of the IEEE Conference on Computer Vision and Pattern Recognition*, pp. 9375–9383 (2019)

10. Hosu, V., Lin, H., Sziranyi, T., Saupe, D.: KonIQ-10k: An ecologically valid database for deep learning of blind image quality assessment. arXiv preprint arXiv:1910.06180 (2019)
11. Huang, Q., Wang, H., Lim, S.C., Kim, H.Y., Jeong, S.Y., Kuo, C.C.J.: Measure and prediction of HEVC perceptually lossy/lossless boundary QP values. In: Data Compression Conference (DCC), pp. 42–51 (2017)
12. Jin, L., Lin, J.Y., Hu, S., Wang, H., Wang, P., Katsavounidis, I., Aaron, A., Kuo, C.C.J.: Statistical study on perceived JPEG image quality via MCL-JCI dataset construction and analysis. *Electronic Imaging* **2016**(13), 1–9 (2016)
13. Kingma, D.P., Ba, J.: Adam: A method for stochastic optimization. arXiv preprint arXiv:1412.6980 (2014)
14. Li, Z., Aaron, A., Katsavounidis, I., Moorthy, A., Manohara, M.: Toward a practical perceptual video quality metric. In: The Netflix Tech Blog, vol. 29 (2016)
15. Lin, H., Hosu, V., Saupe, D.: KADID-10k: A large-scale artificially distorted IQA database. In: 2019 Eleventh International Conference on Quality of Multimedia Experience (QoMEX), pp. 1–3. IEEE (2019)
16. Lin, J.Y., Jin, L., Hu, S., Katsavounidis, I., Li, Z., Aaron, A., Kuo, C.C.J.: Experimental design and analysis of jnd test on coded image/video. In: Applications of Digital Image Processing XXXVIII, vol. 9599, p. 95990Z. International Society for Optics and Photonics (2015)
17. Lin, T.Y., Goyal, P., Girshick, R., He, K., Dollar, P.: Focal loss for dense object detection. In: IEEE International Conference on Computer Vision (ICCV), pp. 2999–3007 (2017)
18. Liu, H., Zhang, Y., Zhang, H., Fan, C., Kwong, S., Kuo, C.C.J., Fan, X.: Deep learning-based picture-wise just noticeable distortion prediction model for image compression. *IEEE Transactions on Image Processing* **29**, 641–656 (2020)
19. Nafchi, H.Z., Shahkolaei, A., Hedjam, R., Cheriet, M.: Mean deviation similarity index: Efficient and reliable full-reference image quality evaluator. *IEEE Access* **4**, 5579–5590 (2016)
20. Recommendation ITU-R BT.500-11: Methodology for the subjective assessment of the quality of television pictures (2002)
21. Redmon, J., Divvala, S., Girshick, R., Farhadi, A.: You only look once: Unified, real-time object detection. In: IEEE Conference on Computer Vision and Pattern Recognition (CVPR), pp. 779–788 (2016)
22. Szegedy, C., Vanhoucke, V., Ioffe, S., Shlens, J., Wojna, Z.: Rethinking the inception architecture for computer vision. In: IEEE Conference on Computer Vision and Pattern Recognition (CVPR), pp. 2818–2826 (2016)
23. Wang, H., Gan, W., Hu, S., Lin, J.Y., Jin, L., Song, L., Wang, P., Katsavounidis, I., Aaron, A., Kuo, C.C.J.: MCL-JCV: a JND-based H. 264/AVC video quality assessment dataset. In: IEEE International Conference on Image Processing (ICIP), pp. 1509–1513 (2016)
24. Wang, H., Katsavounidis, I., Huang, Q., Zhou, X., Kuo, C.C.J.: Prediction of satisfied user ratio for compressed video. In: IEEE International Conference on Acoustics, Speech and Signal Processing (ICASSP), pp. 6747–6751 (2018)
25. Wang, H., Katsavounidis, I., Zhou, J., Park, J., Lei, S., Zhou, X., Pun, M.O., Jin, X., Wang, R., Wang, X., et al.: VideoSet: A large-scale compressed video quality dataset based on JND measurement. *Journal of Visual Communication and Image Representation* **46**, 292–302 (2017)
26. Wiedemann, O., Hosu, V., Lin, H., Saupe, D.: Disregarding the big picture: Towards local image quality assessment. In: International Conference on Quality of Multimedia Experience (QoMEX) (2018)

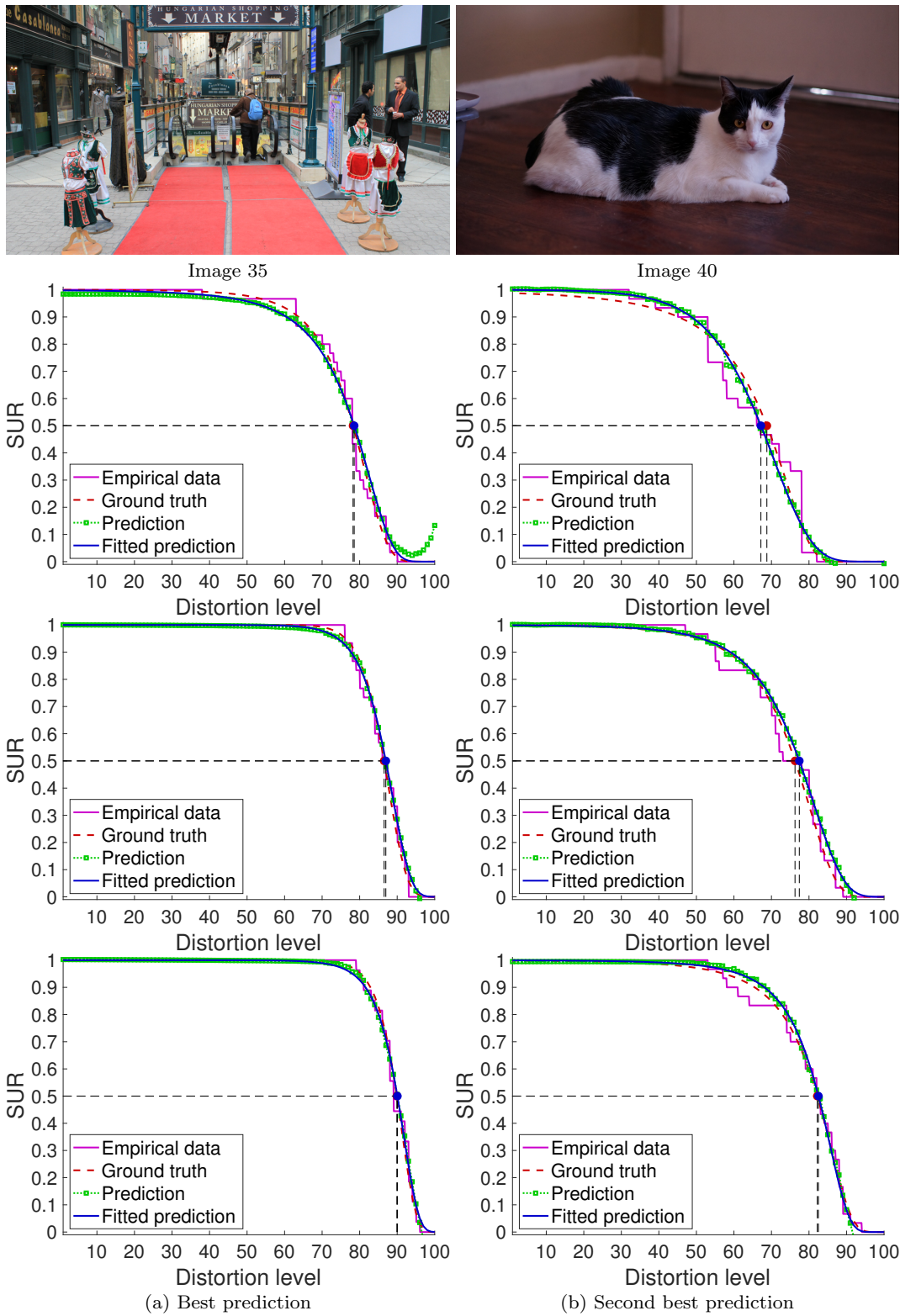


Fig. 6 Best two prediction results according to overall Bhattacharyya distance for the first three JNDs. The first row shows the source images. The second, third, and fourth rows correspond to the first, second, and third JNDs.

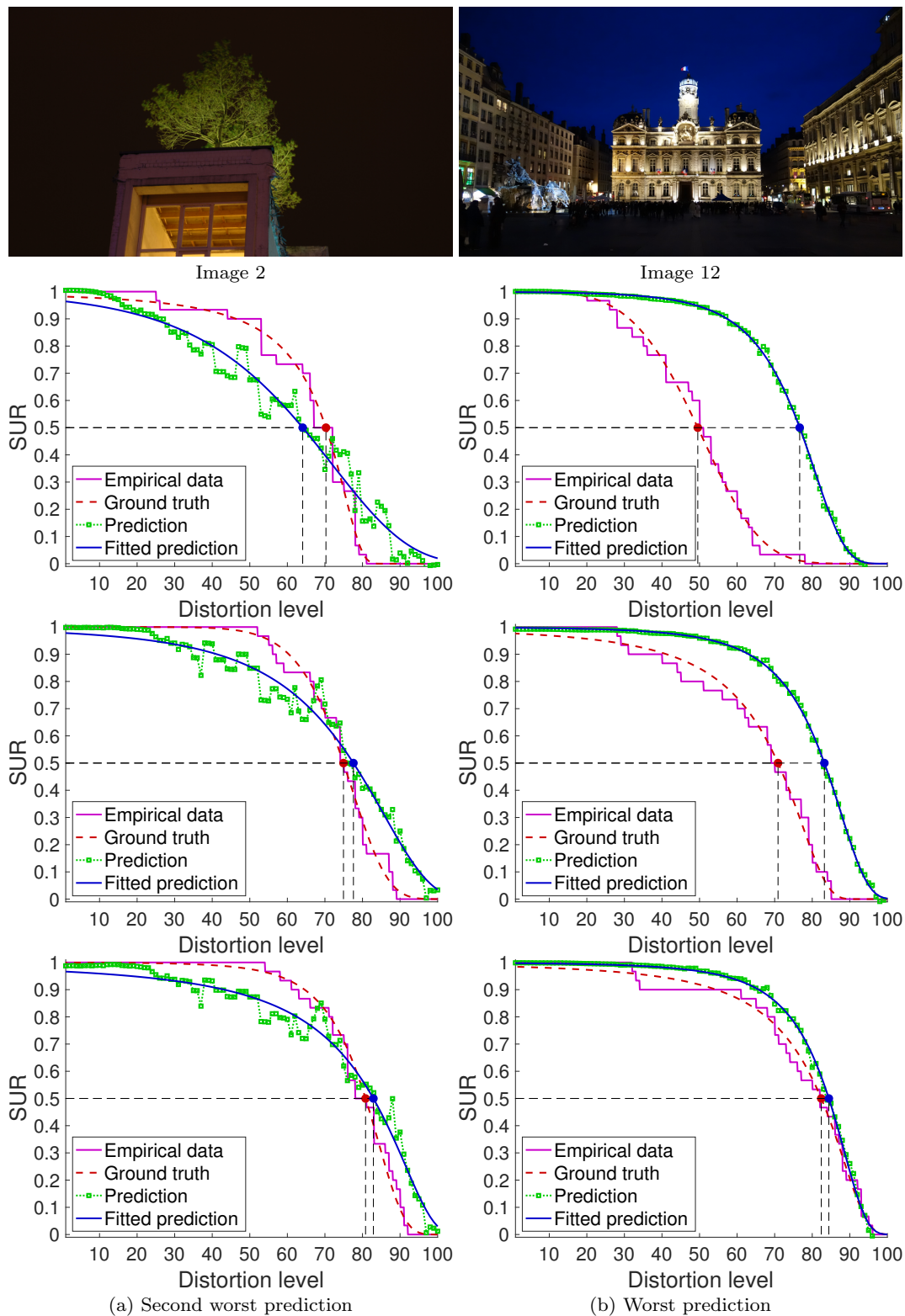


Fig. 7 Worst two prediction results according to overall Bhattacharyya distance for the first three JNDs. The first row shows the source images. The second, third, and fourth rows correspond to the first, second, and third JNDs.

Table 5 GEV distribution model of the *first* JND for the 50 image sequences of the MCL-JCI dataset. Shown are the location μ , scale σ and shape ξ , for both ground truth and SUR-FeatNet, together with the 50% SUR values and PSNR at the 50% SUR value. The Bhattacharyya distance measures the divergence between the predicted and ground truth distributions, $\Delta\text{JND} = |\widehat{\text{JND}} - \text{JND}|$, and $\Delta\text{PSNR} = |\widehat{\text{PSNR}} - \text{PSNR}|$.

Image k	Ground truth					SUR-FeatNet					Bhattacharyya distance	ΔJND	ΔPSNR (dB)
	μ	σ	ξ	JND	PSNR	$\hat{\mu}$	$\hat{\sigma}$	$\hat{\xi}$	$\widehat{\text{JND}}$	$\widehat{\text{PSNR}}$			
1	22.61	6.36	-0.15	76.12	32.08	18.62	7.47	0.25	79.52	31.60	0.0781	3.40	0.49
2	27.82	7.36	0.40	70.27	39.75	29.25	20.88	0.01	64.08	40.80	0.1964	6.19	1.05
3	22.53	8.50	0.28	75.19	31.58	23.73	8.83	0.16	73.94	31.82	0.0105	1.25	0.23
4	21.30	5.36	0.18	77.67	28.90	20.33	8.15	0.11	77.62	28.90	0.0514	0.05	0.00
5	24.29	3.94	0.55	75.11	31.72	24.60	9.22	0.01	73.01	32.00	0.1469	2.10	0.28
6	22.30	4.29	0.73	76.90	33.09	20.35	5.93	0.10	78.43	32.81	0.1476	1.53	0.28
7	31.98	12.22	0.14	64.43	30.00	25.07	9.83	-0.07	72.37	29.12	0.0735	7.94	0.87
8	23.79	3.80	0.29	75.73	28.44	26.35	9.82	-0.05	71.08	28.90	0.1341	4.65	0.47
9	17.53	3.97	0.13	81.98	28.12	20.61	5.37	-0.02	78.43	28.57	0.0444	3.55	0.45
10	21.04	4.08	0.39	78.36	36.63	23.08	10.20	0.14	74.08	37.18	0.1264	4.27	0.55
11	31.15	9.35	-0.19	66.54	34.44	22.24	5.77	-0.07	76.67	33.43	0.1739	10.13	1.02
12	46.97	12.76	-0.22	49.53	34.19	20.98	8.99	0.10	76.66	31.70	0.4884	27.13	2.49
13	21.25	4.97	0.06	77.91	35.53	20.76	7.18	0.18	77.52	35.53	0.0384	0.39	0.00
14	20.79	7.26	0.01	77.54	33.03	19.90	9.48	-0.12	77.70	33.03	0.0216	0.15	0.00
15	20.53	7.65	0.20	77.56	26.55	15.22	5.46	0.11	83.74	25.92	0.0830	6.17	0.63
16	19.66	8.33	0.11	78.23	30.49	21.99	8.00	0.07	76.05	30.73	0.0133	2.18	0.24
17	15.41	5.30	0.23	83.57	28.80	16.38	6.00	-0.01	82.43	28.93	0.0140	1.14	0.13
18	19.42	6.87	-0.29	79.19	33.51	18.34	6.40	-0.03	80.33	33.34	0.0215	1.14	0.17
19	22.18	8.23	-0.17	75.89	29.71	32.46	9.58	-0.05	65.07	30.83	0.1861	10.83	1.12
20	39.41	11.21	-0.70	57.97	32.75	29.75	10.56	-0.17	67.49	31.78	0.1118	9.52	0.97
21	33.01	11.76	-0.40	63.98	29.61	29.53	9.58	0.06	67.92	29.17	0.0552	3.94	0.44
22	20.45	8.65	0.22	77.24	28.75	19.17	8.38	0.12	78.69	28.63	0.0100	1.45	0.12
23	20.13	3.69	-0.01	79.52	26.69	22.23	7.23	-0.00	76.12	27.04	0.0934	3.40	0.36
24	21.03	6.06	-0.06	77.77	32.79	18.98	6.47	0.08	79.61	32.51	0.0181	1.84	0.28
25	21.57	8.27	-0.15	76.48	29.04	15.86	5.82	-0.06	83.04	28.00	0.0826	6.56	1.05
26	39.44	11.83	-1.38	58.16	34.08	30.39	13.27	-0.13	65.86	33.46	0.3194	7.70	0.62
27	15.55	6.61	-0.08	83.07	29.31	16.99	6.77	0.04	81.51	29.64	0.0128	1.56	0.34
28	23.77	6.66	0.36	74.62	39.97	25.07	9.39	-0.13	72.57	40.23	0.0597	2.05	0.25
29	23.07	5.65	-0.01	75.86	36.25	16.32	8.56	-0.18	81.64	35.47	0.1595	5.78	0.78
30	18.90	6.99	0.01	79.53	35.55	16.91	5.57	0.20	81.97	35.12	0.0163	2.44	0.42
31	21.29	7.97	0.03	76.77	33.61	18.85	7.39	0.23	79.32	33.15	0.0151	2.55	0.47
32	22.41	6.81	0.05	76.08	31.12	19.25	5.76	0.12	79.60	30.66	0.0254	3.52	0.46
33	18.43	4.80	0.12	80.77	32.35	23.00	7.47	-0.02	75.28	33.13	0.0647	5.49	0.78
34	26.51	6.51	0.18	72.03	31.40	26.33	7.94	-0.09	71.81	31.52	0.0251	0.22	0.12
35	20.20	6.86	0.09	78.24	30.90	19.55	7.70	0.16	78.54	30.90	0.0073	0.30	0.00
36	20.33	6.70	-0.18	78.29	29.87	21.30	7.25	0.03	77.03	30.00	0.0232	1.26	0.13
37	43.62	19.15	-0.41	50.87	29.89	25.35	8.44	0.13	72.48	27.59	0.2351	21.61	2.30
38	18.27	6.11	0.15	80.43	29.43	18.83	7.68	-0.21	79.46	29.58	0.0356	0.97	0.15
39	21.30	8.13	0.13	76.64	33.90	23.85	8.42	0.06	74.03	34.19	0.0117	2.61	0.30
40	28.79	8.96	0.25	68.78	38.27	30.12	10.12	-0.02	67.19	38.32	0.0187	1.59	0.05
41	16.72	6.21	0.19	81.93	27.35	19.45	7.23	0.10	78.85	27.77	0.0169	3.08	0.43
42	18.13	5.68	0.15	80.73	30.14	22.67	7.66	0.06	75.49	30.84	0.0473	5.24	0.70
43	26.92	8.29	0.19	70.93	35.75	21.44	7.02	-0.21	77.09	34.87	0.1413	6.15	0.88
44	15.25	3.83	0.17	84.30	29.05	16.60	5.07	0.07	82.52	29.41	0.0154	1.79	0.36
45	41.88	15.58	-0.28	53.70	44.54	35.50	11.38	-0.17	61.46	43.64	0.0448	7.76	0.91
46	12.98	5.77	0.10	85.87	31.25	19.46	6.93	0.12	78.94	32.63	0.1235	6.92	1.38
47	24.49	10.31	0.13	72.64	35.39	23.99	8.51	0.10	73.84	35.29	0.0105	1.20	0.10
48	16.81	6.34	0.23	81.77	33.79	23.58	7.46	0.02	74.67	34.95	0.0995	7.10	1.15
49	19.10	6.59	0.18	79.40	36.54	17.36	6.97	0.45	80.86	36.39	0.0245	1.46	0.15
50	15.71	4.53	0.15	83.58	33.41	20.47	6.52	-0.17	78.21	34.43	0.0791	5.36	1.01
Avg.											0.0810	4.53	0.56

Table 6 GEV distribution model of the *second* JND for the 50 image sequences of the MCL-JCI dataset. Shown are the location μ , scale σ and shape ξ , for both ground truth and SUR-FeatNet, together with the 50% SUR values and PSNR at the 50% SUR value. The Bhattacharyya distance measures the divergence between the predicted and ground truth distributions, $\Delta\text{JND} = |\widehat{\text{JND}} - \text{JND}|$, and $\Delta\text{PSNR} = |\widehat{\text{PSNR}} - \text{PSNR}|$.

Image k	Ground truth					SUR-FeatNet					Bhattacharyya distance	ΔJND	ΔPSNR (dB)
	μ	σ	ξ	JND	PSNR	$\hat{\mu}$	$\hat{\sigma}$	$\hat{\xi}$	$\widehat{\text{JND}}$	$\widehat{\text{PSNR}}$			
1	15.32	3.84	-0.22	84.33	30.58	11.24	6.90	0.13	87.17	29.80	0.1977	2.83	0.78
2	22.93	8.70	-0.09	74.94	39.75	17.64	15.26	0.18	77.59	39.07	0.1343	2.65	0.68
3	14.48	4.36	0.33	84.83	30.29	12.87	6.42	-0.05	85.80	30.10	0.0879	0.98	0.19
4	15.17	5.36	0.24	83.78	28.05	14.31	5.99	-0.02	84.51	27.86	0.0278	0.73	0.19
5	17.35	5.52	0.16	81.56	30.78	16.52	7.70	0.03	81.64	30.78	0.0355	0.08	0.00
6	16.24	5.13	-0.13	82.92	32.14	14.69	5.55	0.03	84.26	31.76	0.0186	1.34	0.38
7	21.82	10.98	0.06	75.10	28.76	12.82	7.99	-0.14	85.33	27.33	0.1591	10.23	1.43
8	18.49	3.04	0.27	81.34	27.62	18.67	7.90	0.05	79.41	27.92	0.1520	1.94	0.30
9	12.24	2.51	0.36	87.78	27.03	15.33	5.87	-0.18	83.59	27.82	0.1360	4.19	0.78
10	14.52	3.93	0.03	85.03	35.22	15.23	6.45	0.07	83.37	35.70	0.0490	1.66	0.48
11	22.21	7.18	-0.10	76.21	33.43	15.96	6.26	-0.15	82.81	32.62	0.1113	6.60	0.81
12	26.18	10.06	0.33	70.90	32.41	14.53	8.57	0.17	83.23	30.57	0.2373	12.34	1.84
13	14.00	3.14	0.14	85.83	34.03	14.87	6.07	-0.02	83.92	34.50	0.0747	1.91	0.47
14	12.49	4.93	-0.01	86.70	31.55	13.10	6.83	-0.04	85.42	31.77	0.0213	1.29	0.22
15	11.92	4.37	0.23	87.41	25.37	13.47	5.12	0.23	85.57	25.65	0.0125	1.85	0.27
16	12.75	5.36	0.14	86.23	29.24	12.60	6.58	-0.33	86.13	29.24	0.0604	0.11	0.00
17	11.11	3.74	-0.02	88.52	27.94	10.24	5.04	-0.27	89.00	27.94	0.0390	0.48	0.00
18	12.59	5.18	-0.38	86.64	32.08	14.48	6.84	-0.06	84.04	32.57	0.1072	2.60	0.49
19	15.06	6.79	-0.13	83.51	28.63	18.38	9.16	-0.16	79.36	29.21	0.0398	4.15	0.58
20	25.99	10.56	-0.48	71.46	31.35	20.16	10.21	-0.22	77.25	30.62	0.0497	5.79	0.73
21	21.08	9.85	-0.28	76.49	28.11	19.96	8.09	-0.04	78.10	27.85	0.0188	1.61	0.26
22	11.29	4.04	0.32	88.14	27.12	13.05	6.57	0.22	85.44	27.67	0.0357	2.70	0.54
23	14.87	4.21	-0.05	84.60	25.98	16.93	6.64	0.03	81.62	26.41	0.0557	2.98	0.43
24	15.37	5.89	-0.15	83.53	31.90	13.07	7.35	-0.10	85.29	31.50	0.0306	1.76	0.39
25	12.72	4.69	0.02	86.56	27.42	15.73	7.63	0.26	82.34	28.15	0.0692	4.22	0.73
26	23.66	10.61	-0.32	73.67	32.55	20.34	10.21	-0.16	77.03	32.02	0.0196	3.36	0.54
27	11.13	3.55	-0.04	88.58	28.18	10.52	4.03	-0.16	89.04	27.89	0.0123	0.46	0.30
28	16.23	6.14	0.14	82.46	38.38	16.91	7.81	0.02	81.22	38.65	0.0128	1.24	0.27
29	17.29	4.32	-0.17	82.17	35.30	12.46	6.89	-0.14	86.08	34.44	0.1357	3.91	0.86
30	12.21	5.08	-0.02	86.94	33.85	13.26	5.42	0.01	85.75	34.16	0.0058	1.19	0.31
31	12.90	4.55	0.20	86.37	31.70	9.51	7.10	-0.36	89.05	30.80	0.1596	2.67	0.90
32	13.66	4.22	-0.03	85.80	29.51	10.54	3.84	-0.04	89.06	28.46	0.0695	3.26	1.05
33	11.76	3.97	0.13	87.74	30.83	14.93	7.69	-0.03	83.27	31.79	0.0784	4.48	0.96
34	16.96	5.76	0.17	81.86	30.23	14.30	5.35	-0.09	84.77	29.73	0.0578	2.91	0.49
35	12.87	4.47	-0.08	86.52	29.40	12.22	4.94	-0.00	86.97	29.40	0.0073	0.46	0.00
36	14.66	5.98	-0.06	84.18	28.95	13.52	6.17	0.06	85.19	28.77	0.0080	1.01	0.19
37	28.27	15.47	-0.10	67.16	28.16	19.36	9.31	0.34	78.01	26.83	0.0813	10.84	1.33
38	10.83	3.94	0.14	88.69	27.90	14.54	5.93	0.05	84.26	28.74	0.0620	4.43	0.84
39	11.32	5.73	0.38	87.42	31.72	16.13	5.79	-0.04	82.76	32.82	0.0970	4.66	1.09
40	21.67	8.13	0.12	76.28	37.42	20.32	8.76	0.08	77.42	37.28	0.0091	1.14	0.14
41	10.55	3.71	0.20	89.04	25.83	12.21	5.73	-0.15	86.75	26.51	0.0473	2.29	0.67
42	12.29	4.62	0.05	87.01	28.80	13.25	5.50	-0.01	85.74	29.25	0.0068	1.26	0.45
43	19.54	7.58	0.08	78.64	34.70	14.17	5.92	-0.22	84.74	33.61	0.1475	6.11	1.09
44	9.91	3.67	0.04	89.73	27.86	12.03	5.61	-0.29	87.02	28.40	0.0527	2.71	0.54
45	27.46	12.61	-0.15	69.05	42.56	18.73	11.13	-0.27	78.38	40.90	0.1070	9.34	1.66
46	7.88	4.47	0.12	91.44	29.41	12.10	5.61	0.08	86.82	31.00	0.0745	4.62	1.60
47	14.85	8.63	0.12	82.91	33.83	13.03	4.85	-0.02	86.20	32.91	0.0743	3.29	0.93
48	11.07	6.77	-0.02	87.46	32.33	16.23	6.64	-0.15	82.41	33.59	0.0665	5.05	1.26
49	12.44	6.28	0.05	86.24	35.32	14.00	4.64	0.01	85.29	35.56	0.0399	0.94	0.24
50	10.05	3.95	0.11	89.47	31.60	14.89	5.19	0.03	84.19	33.15	0.1159	5.28	1.55
											0.0702	3.28	0.65

Table 7 GEV distribution model of the *third* JND for the 50 image sequences of the MCL-JCI dataset. Shown are the location μ , scale σ and shape ξ , for both ground truth and SUR-FeatNet, together with the 50% SUR values and PSNR at the 50% SUR value. The Bhattacharyya distance measures the divergence between the predicted and ground truth distributions, $\Delta\text{JND} = |\widehat{\text{JND}} - \text{JND}|$, and $\Delta\text{PSNR} = |\widehat{\text{PSNR}} - \text{PSNR}|$.

Image k	Ground truth					SUR-FeatNet					Bhattacharyya distance	ΔJND	ΔPSNR (dB)
	μ	σ	ξ	JND	PSNR	$\hat{\mu}$	$\hat{\sigma}$	$\hat{\xi}$	$\widehat{\text{JND}}$	$\widehat{\text{PSNR}}$			
1	11.56	3.36	-0.35	88.28	29.51	9.91	5.63	0.09	88.99	29.51	0.1480	0.71	0.00
2	17.34	7.63	0.09	80.82	38.11	13.23	12.34	0.39	82.90	37.73	0.1180	2.08	0.38
3	10.61	4.93	0.04	88.57	29.45	9.44	4.25	0.08	89.98	29.18	0.0077	1.42	0.27
4	11.56	4.60	-0.06	87.78	27.26	11.30	5.18	0.16	87.75	27.26	0.0162	0.03	0.00
5	13.48	5.39	0.10	85.51	30.01	12.06	6.01	0.26	86.63	29.79	0.0182	1.12	0.23
6	11.94	4.17	-0.02	87.53	31.06	10.54	4.65	-0.02	88.76	30.81	0.0182	1.23	0.25
7	16.66	10.38	0.01	80.53	28.10	9.74	5.88	-0.02	89.11	26.57	0.1286	8.58	1.53
8	14.31	4.23	-0.08	85.17	26.98	12.32	5.91	-0.03	86.53	26.79	0.0531	1.36	0.19
9	8.61	2.66	0.20	91.37	26.00	10.07	5.17	-0.15	89.09	26.56	0.0804	2.28	0.56
10	10.59	3.82	0.05	88.99	34.38	10.08	4.88	0.22	89.06	33.98	0.0245	0.07	0.40
11	16.01	6.21	-0.10	82.75	32.62	11.76	4.45	-0.07	87.63	31.74	0.0823	4.88	0.87
12	14.95	9.33	0.34	82.41	30.80	13.72	7.49	0.21	84.42	30.43	0.0167	2.02	0.37
13	10.34	3.04	-0.08	89.56	32.84	10.52	5.13	-0.00	88.60	33.20	0.0675	0.96	0.37
14	8.32	3.27	0.28	91.42	30.24	10.06	4.79	0.00	89.19	30.80	0.0354	2.23	0.56
15	9.13	2.56	0.24	90.89	24.86	10.74	3.59	0.20	88.89	25.22	0.0298	2.00	0.36
16	10.40	3.99	0.06	89.12	28.58	10.68	4.51	0.02	88.66	28.83	0.0028	0.46	0.25
17	10.26	2.74	-0.05	89.74	27.72	9.40	3.14	0.02	90.45	27.49	0.0190	0.71	0.23
18	11.24	3.89	-0.39	88.43	31.53	9.57	6.32	-0.20	89.19	31.19	0.1113	0.76	0.34
19	13.23	5.19	-0.38	86.00	28.27	13.48	5.95	0.10	85.30	28.27	0.0852	0.70	0.00
20	17.46	8.83	-0.21	80.42	30.20	12.63	9.44	-0.18	85.02	29.38	0.0487	4.60	0.82
21	15.69	7.66	-0.08	82.54	27.26	13.28	6.76	-0.05	85.26	26.76	0.0147	2.72	0.50
22	9.32	2.74	0.20	90.64	26.68	9.78	4.75	0.24	89.40	26.90	0.0528	1.24	0.22
23	11.37	4.23	-0.10	88.11	25.31	11.86	5.86	0.01	86.99	25.66	0.0317	1.12	0.35
24	12.73	4.76	-0.16	86.57	31.28	11.03	5.09	-0.01	88.11	30.84	0.0201	1.54	0.44
25	9.85	2.97	0.18	90.02	26.48	10.34	4.83	0.16	88.84	27.00	0.0418	1.18	0.51
26	15.16	7.93	-0.00	82.94	31.23	15.63	7.90	0.07	82.44	31.23	0.0032	0.50	0.00
27	8.69	2.01	0.21	91.55	27.27	8.78	3.17	-0.05	91.07	27.27	0.0491	0.47	0.00
28	11.40	5.15	-0.10	87.75	36.93	13.27	4.67	0.06	86.00	37.59	0.0346	1.75	0.66
29	13.38	4.49	-0.45	86.10	34.44	9.57	5.00	0.02	89.59	33.57	0.1082	3.49	0.87
30	11.24	4.58	-0.32	88.18	33.20	10.01	3.85	0.15	89.54	32.80	0.0527	1.37	0.41
31	8.91	3.49	0.26	90.75	30.42	9.31	4.35	0.07	90.07	30.42	0.0144	0.68	0.00
32	9.99	4.21	-0.01	89.47	28.46	8.49	3.51	-0.11	91.25	27.77	0.0325	1.78	0.69
33	9.31	3.13	0.23	90.49	29.94	11.65	6.30	-0.07	87.07	30.83	0.0835	3.42	0.89
34	12.25	4.66	0.20	86.98	29.35	10.70	4.17	0.03	88.77	28.92	0.0270	1.79	0.43
35	9.71	3.78	-0.01	89.91	28.62	9.40	4.17	0.06	90.06	28.32	0.0052	0.15	0.30
36	12.58	4.51	-0.11	86.80	28.57	11.71	4.52	0.01	87.63	28.35	0.0071	0.83	0.21
37	18.62	13.16	0.09	77.47	26.97	13.64	7.66	0.27	84.41	25.94	0.0548	6.95	1.03
38	8.14	3.00	0.35	91.69	27.06	10.53	5.01	0.01	88.63	27.90	0.0585	3.06	0.84
39	10.50	5.88	0.09	88.31	31.43	12.15	6.15	0.08	86.56	31.99	0.0093	1.75	0.56
40	16.20	6.83	0.19	82.20	36.50	16.19	6.07	0.17	82.51	36.50	0.0043	0.31	0.00
41	9.62	2.48	0.26	90.43	25.57	9.38	4.23	-0.21	90.13	25.57	0.0892	0.30	0.00
42	10.17	4.27	-0.20	89.32	28.28	11.19	4.67	0.15	88.05	28.57	0.0530	1.27	0.29
43	14.69	6.81	-0.05	83.84	33.84	10.34	4.38	-0.08	89.07	32.26	0.1005	5.24	1.58
44	8.53	2.56	-0.05	91.54	27.22	10.37	4.11	0.01	89.12	27.86	0.0721	2.42	0.64
45	17.90	10.94	-0.06	79.14	40.66	13.29	7.33	-0.08	85.06	38.80	0.0651	5.93	1.87
46	8.65	2.98	0.18	91.21	29.41	9.33	4.87	0.04	89.87	30.12	0.0421	1.34	0.71
47	10.53	6.63	0.18	87.95	32.62	9.70	4.32	-0.07	89.74	31.96	0.0589	1.78	0.66
48	8.27	4.37	0.26	91.05	30.86	11.51	4.91	0.00	87.69	32.33	0.0537	3.36	1.47
49	8.84	3.15	0.49	90.89	34.12	10.89	3.65	-0.04	88.78	34.82	0.0642	2.11	0.70
50	8.46	2.92	0.25	91.42	30.77	13.32	4.06	0.08	86.17	32.59	0.1956	5.25	1.82
											0.0522	2.07	0.53